

Plant Taxonomy Meets Plant Counting: A Fine-Grained, Taxonomic Dataset for Counting Hundreds of Plant Species

Jinyu Xu, Tianqi Hu, Xiaonan Hu, Letian Zhou, Songliang Cao, Meng Zhang, Hao Lu*
 Huazhong University of Science and Technology, China
 {jinyu_xu, hlu}@hust.edu.cn

Abstract

Visually cataloging and quantifying the natural world requires pushing the boundaries of both detailed visual classification and counting at scale. Despite significant progress, particularly in crowd and traffic analysis, the fine-grained, taxonomy-aware plant counting remains underexplored in vision. In contrast to crowds, plants exhibit nonrigid morphologies and physical appearance variations across growth stages and environments. To fill this gap, we present TPC-268, the first plant counting benchmark incorporating plant taxonomy. Our dataset couples instance-level point annotations with Linnaean labels (kingdom→species) and organ categories, enabling hierarchical reasoning and species-aware evaluation. The dataset features 10,000 images with 678,050 point annotations, includes 268 countable plant categories over 242 plant species in Plantae and Fungi, and spans observation scales from canopy-level remote sensing imagery to tissue-level microscopy. We follow the problem setting of class-agnostic counting (CAC), provide taxonomy-consistent, scale-aware data splits, and benchmark state-of-the-art regression- and detection-based CAC approaches. By capturing the biodiversity, hierarchical structure, and multi-scale nature of botanical and mycological taxa, TPC-268 provides a biologically grounded testbed to advance fine-grained class-agnostic counting. Dataset and code are available at <https://github.com/tiny-smart/TPC-268>.

1. Introduction

High-quality datasets such as PASCAL VOC [12], ImageNet [9], and COCO [27] have driven vision studies in classification, detection, and segmentation for decades. A similar line also appears in visual counting [5], a task aiming to count objects in extreme clutter and occlusion. Interestingly this field is dominated by the study of rigid objects like crowds [56] and vehicles [20]. Consequently, most

*Corresponding author.



Figure 1. **Counting plants versus counting generic objects.** Plants inherently exhibit rich biodiversity, fine-grained variations, non-rigid structures, and time-space variations, which collectively create a nonnegligible gap against generic objects.

technical improvements are overfitted into these types of objects, rendering poor generalization when counting other categories in the natural world, plants for instance.

Plant counting is not merely a niche application of existing counting approaches [34]; it represents a fundamentally distinct and more demanding set of challenges. As shown in Fig. 1, unlike crowds, where individuals often share similar appearance that can provide informative contextual cues [6], plants exhibit staggering diversity and complexity. They are non-rigid, undergo dramatic morphological changes during their life cycle, and is highly sensitive to environmental factors—a concept known as phenotypic plasticity [54]. This task is thus not simple single-class

counting, but *fine-grained instance counting across a vast and hierarchically structured class space*. For example, a crowd counting model only requires distinguishing “person” from “background”, but a plant counting system must learn the subtle textural differences to separate hundreds of species, a problem more akin to fine-grained visual categorization [50] but at a massive scale of instance density. This unique intersection of large-scale counting and fine-grained, taxonomy-aware recognition has been largely overlooked by the vision community. A possible reason may be due to the lack of a suitable benchmark.

To this end, we introduce TPC-268, the first large-scale, plant-orientated counting dataset that explicitly integrates plant taxonomy. Substantially larger than prior plant counting datasets introduced in plant science [8, 13, 18, 26, 34], TPC-268 comprises 10,000 images, featuring 678,050 point and 30,000 bounding box annotations. It covers a remarkable diversity of life, including 242 plant species, organized into 268 distinct biological organization-level countable categories (*e.g.*, different organs of the same species are treated as separate counting categories). A key feature of this dataset is its deep integration of plant taxonomy. Unlike generic objects, plants possess inherent, systematic priors encoded in their evolutions. We annotate each instance with its full taxonomic hierarchy (from kingdom to species), transforming the counting problem into *joint counting and hierarchical reasoning*. This rich, structured information allows the vision community to investigate not only how visual representations learned at one taxonomic level (*e.g.*, family) can generalize to unseen species within it, but also how shared visual traits correspond to phylogenetic closeness. This explicit encoding of biological structure provides a principled framework for developing robust and generalizable category-agnostic counting models. Furthermore, we provide multi-level annotations (Fig. 2) that decompose plants into differing organizations (*e.g.*, tissues, organs, whole plants, and canopies), enabling the study of cross-species understanding of homologous structures and model generalization across vast changes in observation scale, from macroscopic canopies to microscopic stomata.

The sheer taxonomic scale of the plant kingdom renders the conventional ‘one-model-per-species’ paradigm fundamentally unscalable. This reality motivates us to frame plant counting as a Class-Agnostic Counting (CAC) problem, where the goal is to learn the general concept of “how to count” given visual exemplar(s). Doing so not only aligns with the practical need of plant science but also establishes a new, complex frontier for CAC research, which necessitates a principled methodological and experimental design to navigate. A core principle of our dataset design is a strict, taxonomy-aware evaluation of generalization. Unlike existing benchmarks, our data splits are defined at the species-organization level, guaranteeing that a model tested on, for

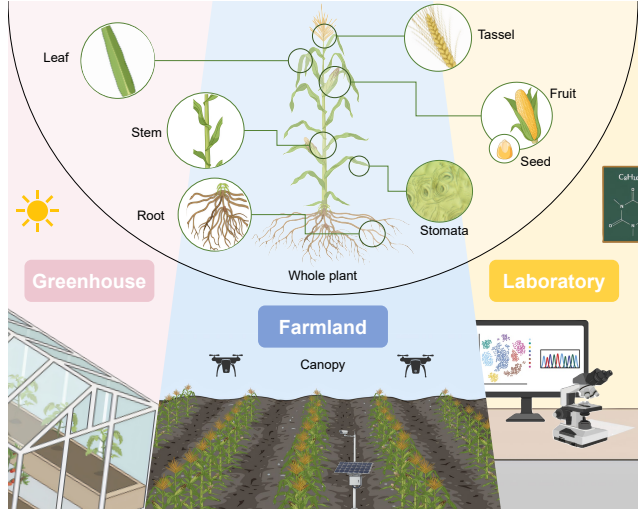


Figure 2. **Distinct organization-level countable plant categories across multiple observation scales and environments in the TPC-268 dataset.** Our TPC-268 covers four organization levels including tissue, organ, organism, and population, spans across various observation scales (ranging from microscopy and close-range photography to UAV imagery), and hosts 268 countable categories (such as leaves, stems, and fruits) under heterogeneous environments (from laboratory to field).

example, an “*Oryza sativa* leaf” has never seen any leaf from the entire *Oryza* genus during training. This methodology allows us to rigorously benchmark how a model generalizes across a true, biologically-defined taxonomic gap—a far more challenging and realistic measure of zero-shot counting. Under this strict protocol, we provide a comprehensive benchmark of state-of-the-art CAC approaches, systematically analyzing how different architectural priors tackle the unique challenges posed by our dataset, from fine-grained distinctions to extreme scale variations (Fig. 2). By grounding the class-agnostic challenge in a biologically meaningful hierarchy and providing this rigorous evaluation framework, TPC-268 serves as a new, challenging testbed to spur innovation in fine-grained visual counting.

2. Related Work

Our work is related to single-image counting datasets, plant counting, and class-agnostic counting.

Single-Image Counting Datasets. Counting datasets have evolved from class-specific to class-agnostic ones. Table. 1 compares main counting datasets introduced in the vision community over the past decade. It can be observed that early work [22, 46, 56] focuses on a single category in dense scenarios, primarily targeting crowds where severe occlusions and perspective changes pose major challenges. Subsequent work expands to other domains such as cells [38], animals [2, 47], leaves [40], and vehicles [20].

Table 1. **Representative visual counting datasets introduced by the computer vision community in the past ten years.**

Dataset	Venue	#Images	#Labeled Instances	Avg. Resolution	Target	#Classes
ShanghaiTech A [56]	CVPR'16	482	241,677	868×589	Crowd	1
ShanghaiTech B [56]	CVPR'16	716	88,488	1024×768	Crowd	1
Penguin dataset [2]	ECCV'16	80,095	575,082	1920×1080	Penguin	1
CARPK [20]	ICCV'17	1,448	89,777	1280×720	Car	1
CVPPP [10]	ICCVW'17	1,311	18,016	842×812	Leaf	1
DCC [38]	CVPR'18	177	6,036	256×256	Cell	1
UCF-QNRF [22]	ECCV'18	1,535	1,251,642	2902×2013	Crowd	1
JHU-CROWD++ [46]	TPAMI'20	4,375	1,515,005	1430×910	Crowd	1
NWPU-Crowd [52]	TPAMI'20	5,109	2,133,375	3209×2191	Crowd	1
IOCFish5K [47]	CVPR'23	5,637	659,024	1920×1080	Fish	1
FSC-147 [43]	CVPR'21	6,135	344,150	523×384	Miscellaneous	147
FSCD-LVIS [41]	ECCV'22	6,196	402,945	586×479	Miscellaneous	377
Mara-Wildlife [24]	CVPR'24	1,012	28,146	8256×5504	Animal	21
TPC-268	This work	10,000	678,050	1130×959	Plant	268

A limitation of these datasets is the expensive annotation cost, as a single image can contain thousands of annotations, impeding scalability to new scenarios and categories. This bottleneck motivates a paradigm shift toward CAC [33], which reframes the objective from learning what to count to learning how to count. However, the practical success of this paradigm hinges on the diversity and granularity of the underlying benchmarking data. Existing CAC datasets [41, 43] lack the fine-grained categorical complexity found in many real-world domains. While effort such as WildLife-Mapper [24] has begun to address this gap for wildlife counting, the more challenging plant kingdom remains underexplored. To date, the community still lacks a large-scale, fine-grained counting dataset.

Plant Counting. Plant counting is a statistical approach primarily used and developed by experts in plant science and agriculture to link genotypes with plant phenotypes [14]. It underpins various agricultural tasks, including emergence rate, biomass and yield estimation in breeding trials. Early methods, mostly driven by the plant science community, relied on sensors [11, 36], digital image processing techniques [16] with tools like ImageJ [44] and SmartGrain [48]. Yet, these approaches suffer from reliance on manual feature engineering and are sensitive to environmental variations. Only until recently, deep-learning based approaches are introduced in plant counting [3, 15, 34], significantly accelerating the iteration of plant counting techniques. Albeit effective, these approaches can only count specific plant species. Once the counting category changes, a repetitive loop of data collection, annotation, and model retraining is required. This tedious workflow yields a collection of multiple yet isolated species-specific plant counting datasets. To address this limitation and catalyze more generalizable plant counting approaches, we construct a novel plant counting dataset, TPC-268, featuring a hierar-

chical taxonomic structure for plant-agnostic counting.

Class-Agnostic Counting. Conventional counting methods can only count predefined categories, such as crowds [56], vehicles [20], and cells [19]. To mitigate this category dependency, CAC is introduced to generalize a counting model for unseen categories. CAC is a typical exemplar-to-image semantic correspondence problem [28, 31, 45, 53, 55]. With several predefined exemplars as input, they are matched with the image to search visually similar content, and the density map is used to encode the object count. To improve output interpretability, [41] marries CAC with detection. This detection-based paradigm directly locates and counts instances with bounding boxes. Besides these exemplar-guided approaches, a text-guided paradigm also emerges, which uses text prompts for open-set object counting [32]. Across these paradigms, while the conditioning signal may differ, their goal remains the same: counting instances of a user-specified, novel concept at test time. In this work, we extend the problem connotation of CAC in the plant counting domain and curate a plant counting benchmark with point-level annotations to assess generalization across taxonomic and fine-grained plant species.

3. Taxonomic Plant Counting Dataset

Here we introduce our benchmark, TPC-268, a large-scale taxonomic plant counting dataset, present its hierarchical taxonomic structure, and provide its statistics.

3.1. Plant Taxonomy Meets Plant Counting

We highlight plant taxonomy for plant counting. Plant taxonomy organizes species as a nest hierarchical ranks: Kingdom, Phylum, Class, Order, Family, Genus, and Species. In this structure, higher-level ranks (*e.g.*, class, order, family) group plants that share broad mor-

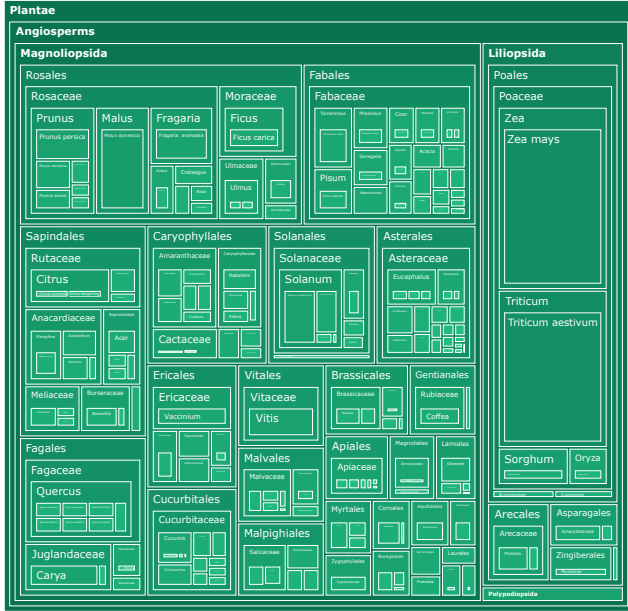


Figure 3. **Treemap of plant taxonomic hierarchy in TPC-268.** Each nested rectangle represents a specific taxonomic rank, from Kingdom (Plantae), Phylum (e.g., Angiosperms), Class (e.g., Magnoliopsida, Liliopsida), Order (e.g., Rosales, Poales), Family (e.g., Rosaceae, Poaceae), Genus (e.g., Prunus, Zea), to Species (e.g., Prunus persica, Zea mays). Box area represents the number of images for that taxonomic unit.

phological and ecological patterns such as growth form, leaf and stem architecture, or reproductive structures, while lower-level ranks (e.g., genus and species) distinguish subtler phenotypic differences among closely related taxa, providing a structured similarity potential for visual cues. Building on this observation, we make counting explicitly taxon-aware by embedding each counting instances into the Linnaean hierarchy [29], rather than treating the species as unrelated categoric labels. The annotation can thus be interpreted and aggregated at multiple taxonomic levels (e.g., species-level vs. genus- or family-level counts), and category splits can be defined in terms of taxonomic distance. With this taxonomic annotation available, a model can be encouraged to generalize from seen specie to unseen but taxonomic related species.

3.2. Dataset Collection

The dataset integrates curated public resources with controlled data collection to achieve broad taxonomic coverage and data reliability. Major sources are distributed among Wikipedia (34%), *PlantCLEF* (29%) [39], Internet (14%), Tree Leaf Stomata (11%) [51], *MTC-UAV* (3%) [35], *CVPPP* (3%) [10], *CKC-Wild* (3%) [25], and others (3%). All data undergoes a rigorous preprocessing pipeline to filter out samples unsuitable for counting, with annotations being manually refined or newly created to ensure quality.

The dataset spans scales from tissue-level microscopy to canopy-level UAV imagery. Collected across laboratories, greenhouses, and natural habitats, the images include variations in illumination, background, and occlusion, alongside common degradations such as blur and compression.

The dataset encompasses extensive geographical and ecological diversity across Asia, Africa, *etc.* covering ecosystems from tropical to alpine environments. It incorporates major crops such as *Oryza sativa*, and *Zea mays*, alongside specialized arid-zone plants like *Acacia tortilis*.

The dataset also incorporates ecologically rare, geographically restricted, and conservation-significant taxa. Examples include the critically endangered *Arenaria paludicola*, near-threatened *Boswellia sacra*, and regionally endemic *Jacobaea taitungensis* and *Nubelaria arisanensis*. These species are validated against the IUCN Red List [30].

The deliberate inclusion introduces a naturally long-tailed distribution across both taxonomic and morphological dimensions, providing a valuable testbed for studying model robustness and hierarchical generalization under extreme sample imbalance and ecological rarity.

Image sources comply with copyright licenses. Sensitive geographical metadata is anonymized and used solely for ecological stratification to protect privacy.

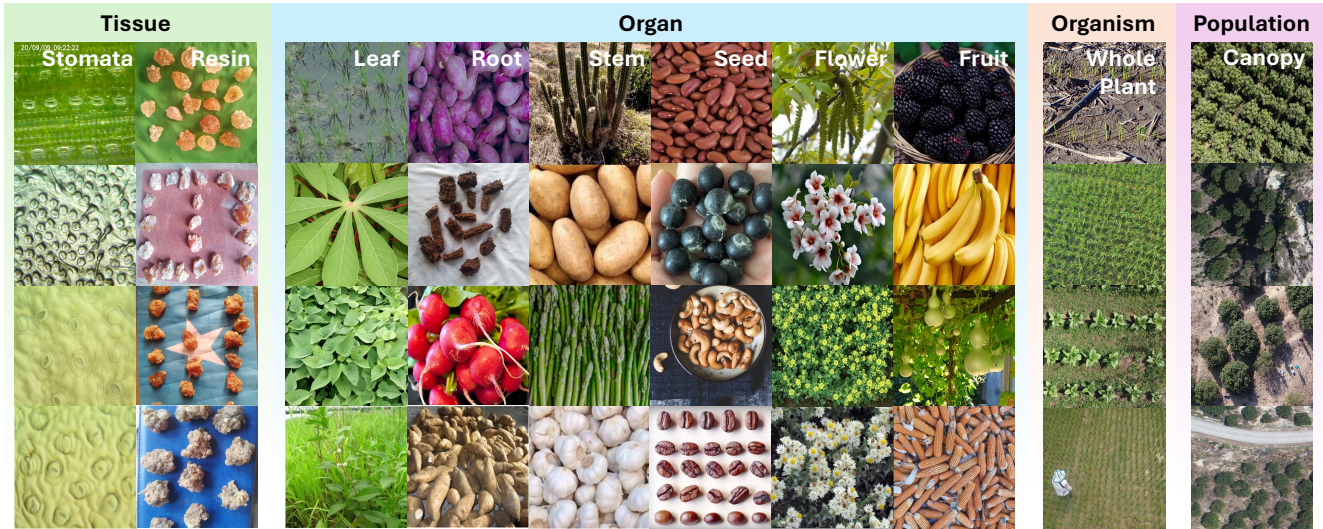
3.3. Annotation Protocols

Our annotation strategy is designed to capture both the instance location for counting and the taxonomic identity for hierarchical analysis.

Annotation of Instance and Exemplar. We adopt the standard point-box protocol in CAC [43], providing point annotations at the structural center of each instance and bounding boxes for three instances per image. For partial occlusion, we follow a *visible-shape dominance* principle, annotating only visible structures. Box exemplars are selected to cover: i) representative appearance, ii) diverse scales, and iii) morphological or environmental variations.

Annotation of Taxonomy and Biological Organization. A key feature of our dataset is its complete taxonomic hierarchy. Each image is linked to the full Linnaean taxonomy [29] of its primary species. In practice, we used *Pl@ntNet* [23] for initial genus-species identification, completed the remaining hierarchy using the *World Flora Online* database [4], and subjected all data to rigorous manual verification. Annotators cross-referenced identified species with *Pl@ntNet*'s organ-specific images; all labels underwent a 3-round human check. Finally, each species' position is encoded as a 7-dimensional vector. A complete mapping table can be found in the supplementary. For example, *Malus domestica* is encoded as [1, 1, 1, 14, 39, 113, 136].

Biological organization information (e.g., stomata, flower, and whole plant) is also included as auxiliary meta-



(a) Ten countable categories across four biological organizations in TPC-268

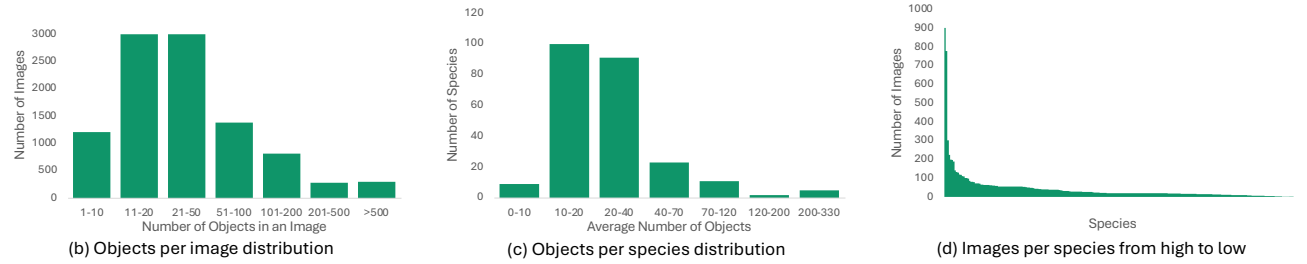


Figure 4. **Examples and statistical distributions of TPC-268.** The figure illustrates (a) representative samples of ten countable plant categories across four biological organizational levels. The associated statistical distributions show (b) the number of objects per image, (c) the number of objects per species, and (d) the number of images-per-species.

data, and its distribution across ten major categories is detailed in Fig. 4(a). This metadata specifies the type of biological structure depicted in the image. Specifically, for multi-organ handling, images with distinct multiple organs (e.g., flowers and fruits) are annotated as separate categories with specific suffixes, whereas indiscernible cluttered regions are treated as background. This label is critical for vision tasks, as the visual features (e.g., texture, shape, color) of the same species vary dramatically depending on the structure shown (e.g., a *Malus domestica* “leaf” image versus its “whole plant” image). This information thus helps to horizontally categorize different plant varieties based on the specific biological structure depicted, not just by species. Fig. 5 shows an example of annotation.

Annotation Pipeline. Our annotation pipeline combines public data sources with newly created labels. Annotations for approximately 80% of the images were created from scratch by a professional annotation team over three months. For the remaining images with existing bounding boxes, we extracted box centers as points. Subsequently, all annotations (new and sourced) undergo a rigorous three-round review by researchers experienced in plant phenotyp-

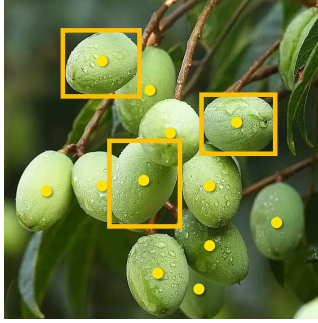
ing to ensure accuracy, particularly for complex cases like overlapping organs and dense regions.

3.4. Dataset Partition

To enforce strict category independence between subsets, we partition the dataset based on taxonomic identity and visual characteristics (e.g., observation scale and density).

The minimal indivisible unit (category) is defined as a species–organization pair (e.g., *Triticum aestivum*–flower vs. *Triticum aestivum*–stomata). Each pair is treated as an independent category and is assigned to one subset (train, val, or test), preventing any instance overlap between different sets. We formulate the partition as a multi-objective optimization problem and solve it using a Mixed-Integer Linear Programming (MILP) model with three constraints: i) scale coverage: each split must include at least one instance from every observation scale (microscopy, close-up, and remote sensing); ii) density balancing: the average number of points per image should maintain balanced across all subsets; and iii) ratio adherence: an approximate 7:1:2 split for training, validation, and testing.

This split achieves a balanced average density of 67.81



Instances:
12 points

Exemplars:
3 boxes

Taxonomy:
Plantae-Tracheophyta-
Magnoliopsida-Sapindales-
Burseraceae-Canarium-Album

Biological Organization:
Organ-Fruit

Figure 5. **An annotation example.** Each sample contains annotations for instances, exemplars, taxonomy, and organization.

instances per image across all subsets. The MILP-based approach ensures that, while the splits are taxonomically distinct, they remain statistically balanced in instance density and observation scale coverage. Further details w.r.t. the MILP-based partition can refer to the supplementary.

3.5. Statistics and Analysis

The TPC-268 dataset contains 10,000 images, including annotations of 678,050 points and 30,000 bounding boxes.

Distribution of Density. Instance counts range from 5 to 1,462 with a long-tailed distribution (median: 25.0; 75-th percentile: 58.0; 90-th percentile: 129.0). 72.1% of images contain fewer than 50 instances, 22.0% contain between 50 and 200, and 3.0% exceed 500, as visualized in Fig. 4(b).

Hierarchical Taxonomic Structure. The dataset follows the Linnaean system, including 2 kingdoms, 2 phyla, 4 classes, 35 orders, 83 families, 192 genera, and 242 species. Long-tailed distributions persist across all ranks. At the family level, the mean image count (121.9) exceeds the median (40). Ranked by image count, the top 10 families, genera, and species account for 60.9%, 38.9%, and 32.0% of images, respectively. 53.5% of species contain fewer than 20 images, and 8.3% contain 5 or fewer. This species-level skew is illustrated in Fig. 4(c) and Fig. 4(d).

Biological Organization and Scale. The dataset spans four organizational levels: tissue (1,096 stomata, 228 resin), organ (4,422 fruit, 2,994 flower, 602 seed, 196 stem, 118 root, 74 leaf), organism (214 whole plant), and population (56 canopy). Observation scales range from microscopic structures (165×127 pixels) to macroscopic canopy-level drone imagery ($6,000 \times 4,000$ pixels). Fig. 4(a) provides the corresponding example images.

4. Results and Discussion

In this section, we conduct comprehensive experiments to assess the proposed TPC-268 benchmark from multiple perspectives. We benchmark a wide range of representative CAC approaches under a unified evaluation set-

ting, encompassing both regression-based and detection-based paradigms. Furthermore, we investigate cross-dataset transfer to analyze the domain discrepancies between plant counting and generic object counting.

4.1. Experimental Setup

We evaluate our dataset under the standard exemplar-based CAC paradigm, where each test image is accompanied by K exemplar patches cropped from the original image. Following existing CAC approaches [33], we consider both the *3-shot* and *1-shot* settings. For cross-dataset transfer, we train models separately on TPC-268 and FSC-147, and evaluate the performance on another dataset.

We benchmark both regression-based and detection-based CAC frameworks. Regression-based methods follow the exemplar-to-density paradigm, where the model takes an image and exemplar prompts as input to predict a density map. We include: 1) FamNet [43], SAFECount [55], and BMNet+[45]: CNN-based works that establish the feature matching and density regression framework; 2) SPD-CNet [28]: a CNN-based model utilizing scale-prior deformable convolutions; 3) CountTR [31] and CACViT [53]: transformer-based approaches that leverage self-attention to capture global context; 4) LOCA [49]: a strong baseline that incorporates local similarity matching and scale-adaptive modules; 5) DAVE [42]: a two-stage detect-and-verify framework; 6) TasselNetV4 [21]: a vision foundation model for cross-scene, cross-scale, and cross-species plant counting. Detection-based methods reformulate counting as an exemplar-guided detection task, providing instance-level localization. We consider: 1) C-DETR [41]: a DETR-based model that directly predicts bounding boxes for all instances similar to the exemplars; 2) CountGD [1]: a recent method that uses Gaussian heatmaps for instance localization. This selection ensures a balanced comparison across different architectures (CNN vs. Transformer) and output representations (density maps vs. bounding boxes), providing insights into which paradigm is more suitable for plant counting.

4.2. Benchmark Results

Main results on TPC-268 are shown in Table. 2. Note that each image in our dataset has 3 visual exemplars. For the *1-shot* setup, we randomly select one and report the standard deviation. For *3-shot*, since all exemplars are used, no test-time randomness is introduced, therefore no standard deviation. Overall, regression-based models outperform detection-based models. This indicates that explicit object localization is hindered by the compact spatial arrangement and structural entanglement present in our dataset.

Within the regression-based models, LOCA achieves the best performance on the test set, surpassing both CNNs and Transformer designs, suggesting that integrating local structure cues with global context modeling effectively captures

Table 2. Comparison with the state-of-the-art CAC approaches on the TPC-268 dataset. Best performance is in boldface.

Method	Venue & Year	Backbone	Shot	Val			Test		
				MAE↓	RMSE↓	R^2 ↑	MAE↓	RMSE↓	R^2 ↑
FamNet [43]	CVPR'21	R50	3	28.87	52.51	0.58	30.43	65.62	0.62
BMNet+ [45]	CVPR'22	R50	3	29.33	77.78	0.47	27.78	57.25	0.50
C-DETR [41]	ECCV'22	R50	3	22.66	77.51	0.75	22.68	57.97	0.74
SPDCNet [28]	BMVC'22	R18	3	25.66	72.49	0.52	23.70	47.53	0.64
CountTR [31]	BMVC'22	Hybrid	3	20.21	55.82	0.73	25.19	49.94	0.62
SAFECount [55]	WACV'23	R18	3	22.57	63.65	0.64	25.70	52.30	0.58
LOCA [49]	ICCV'23	R50	3	17.26	53.19	0.75	17.51	38.37	0.78
DAVE [42]	CVPR'24	R50	3	16.47	52.87	0.76	17.61	40.06	0.75
CACViT [53]	AAAI'24	ViT-B	3	16.63	42.49	0.82	22.04	41.79	0.73
CountGD [1]	NeurIPS'24	Swin-B	3	18.32	54.55	0.74	19.52	50.51	0.61
TasselNetV4 [21]	ISPRS'26	ViT-B	3	13.20	43.93	0.83	22.95	51.36	0.60

FamNet [43]	CVPR'21	R50	1	33.11±0.68	68.95±4.15	0.58±0.05	33.63±1.13	62.07±2.94	0.41±0.05
BMNet+ [45]	CVPR'22	R50	1	29.33±0.13	77.50±0.31	0.48±0.05	27.84±0.10	56.98±0.12	0.50±0.01
CountTR [31]	BMVC'22	Hybrid	1	20.16±0.05	55.15±0.82	0.73±0.01	25.19±0.14	50.23±0.24	0.62±0.00
LOCA [49]	ICCV'23	R50	1	17.19±0.31	48.14±2.19	0.80±0.02	21.47±0.29	42.36±0.72	0.73±0.01
DAVE [42]	CVPR'24	R50	1	16.06±0.60	48.35±1.19	0.80±0.01	19.47±0.44	42.54±0.35	0.72±0.00
CACViT [53]	AAAI'24	ViT-B	1	17.96±0.16	43.38±0.47	0.83±0.00	22.06±0.11	42.97±0.81	0.71±0.01
TasselNetV4 [21]	ISPRS'26	ViT-B	1	13.49±0.02	41.30±0.46	0.85±0.00	22.20±0.11	48.70±0.26	0.67±0.00

Table 3. Results of cross-dataset transfer. $A \rightarrow B$ denotes model trained on dataset A and tested on the test set of dataset B. Red/Blue indicate MAE increase/decrease compared to training and testing on the same dataset ($A \rightarrow A$).

Method	FSC-147→FSC-147			FSC-147→TPC-268			TPC-268→TPC-268			TPC-268→FSC-147		
	MAE	RMSE	R^2	MAE	RMSE	R^2	MAE	RMSE	R^2	MAE	RMSE	R^2
CountTR [31]	11.90	90.88	0.62	38.62 (+225%)	75.78	0.12	25.19	49.94	0.62	26.53 (+5%)	126.25	0.26
CACViT [53]	10.83	73.12	0.75	26.73 (+147%)	103.35	-0.63	22.04	41.79	0.73	17.88 (-19%)	82.57	0.68
LOCA [49]	10.72	56.10	0.85	24.70 (+130%)	68.68	0.59	17.51	38.37	0.78	15.16 (-13%)	109.15	0.45

fine morphological details and dense overlapping present in the dataset. In contrast, models relying primarily on global self-attention, such as CACViT and TasselnetV4, demonstrate strong validation performance but generalize poorly to unseen scenes in test. Since most baselines show negligible val-test differences, this gap originates from the approach per se rather than data sampling. During parameter selection, these global models tend to select hyperparameters that overfit the validation data. TasselNetV4 still demonstrates strong overall performance and higher R^2 scores on the validation split, showing that global interaction is beneficial for density estimation. However, its performance gap on the test set suggests that the species variation and structural diversity present in the dataset challenge purely global feature reasoning. This highlights that capturing local structural consistency is essential for robust generalization across species and imaging conditions.

For detection-based approaches, C-DETR and CountGD perform markedly worse than regression models. Their

poor performance arises from distinguishing individual instances under severe occlusion and high morphological similarity. This indicates that our dataset benefits more from holistic estimation than explicit instance localization.

We visualize test samples via t-SNE [37], using 256-dimensional feature vectors computed as the mean of their LOCA [49] prototypes. The results are shown in Fig. 6, where the features are grouped and colored by Order-level taxonomy (left) and organization structure (right). Results reveal that samples sharing the same label fail to form well-separated clusters under either scheme. This confirms that the learned features lack clear class-level distinctions, and the SOTA method is insufficient to capture deep biological characteristics when relying solely on visual information.

4.3. Fine-Grained Performance Evaluation

A fine-grained evaluation of LOCA reveals distinct performance variations across taxonomic, scaling, and data dimensions. Taxonomic analysis shows that errors in *Bras-*

Table 4. **Performance of CountGD on the TPC-268 test set with different prompts.** The species and taxonomic information are provided in text.

Target Specification	MAE↓	RMSE↓	R^2 ↑
3 visual exemplars	19.52	50.51	0.61
+ species name	17.53	44.80	0.69
+ full taxonomy	16.90	43.32	0.71

sicaceae (MAE 62.4) and *Poaceae* (54.7) exceed those in *Rosaceae* (14.1), with *Brassica* (141.5) and *Zea* (67.4) being the primary error sources due to their extreme densities (228.2 and 172.3) and severe occlusion. Across observation scales, LOCA excels in microscopic settings (MAE 3.71) but struggles in macroscopic (20.30) and aerial (15.87) views. For high-density samples (> 100), microscopic error remains low (5.9) while macroscopic error spikes (53.7), implying robustness to repetitive patterns but sensitivity to complex spatial occlusions. The weak correlation between sample quantity and error (Pearson $r = 0.32$) further confirms that counting difficulty is intrinsically tied to morphological complexity rather than data scale.

4.4. Cross-Dataset Transfer

Table 3 reports the performance of three models on cross-dataset setting. A key observation is the substantial performance degradation across all models when trained on FSC-147 and tested on TPC-268, indicating that the model trained on generic objects struggle to generalize to plants. Conversely, when the training and testing datasets are exchanged, the MAE shows negligible increases or even reductions. This indicates that our plant counting dataset is a more challenging task than FSC-147 and the model trained on TPC-268 can generalize to generic objects naturally. We note that the RMSE and R^2 metrics exhibit more pronounced performance degradation, which is expected as these metrics are more sensitive to the large errors and outliers common in challenging domain adaptation scenarios.

4.5. Insights into Taxonomic Information

To validate the utility of the proposed hierarchical taxonomic annotations, we retrain CountGD [1] by incorporating taxonomic information as textual descriptions. Compared with the visual-exemplars-only setting, in the species-level experiment we add a text prompt containing the species name. For the full taxonomy setting, the text prompt is in the format: “*Kingdom, Phylum, Class, Order, Family, Genus, Species.*” The models are retrained and evaluated under these configurations. As shown in Table 4, this consistent improvement confirms that structured biological knowledge provides a practical inductive bias for the task.

We further evaluate the impact of taxonomy on LOCA using unseen categories. For genus transfer, unseen species

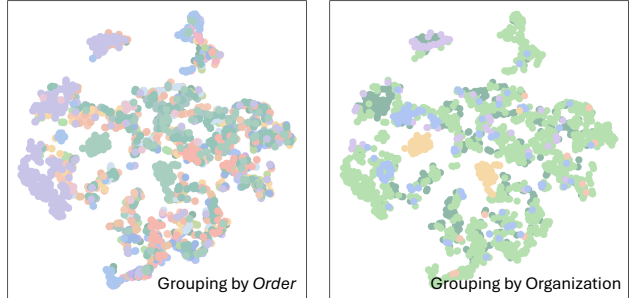


Figure 6. **t-SNE visualization of LOCA [49] prototype features on the test set.** Different colors indicate different groups.

of *Quercus* achieve low test MAEs (3.79, 3.62) by benefiting from related *Quercus* training samples. In contrast, the taxonomically isolated *Litchi chinensis* suffers a higher error (15.61) despite comparable density. Similarly, in cross-organ evaluation, *Ricinus communis* (trained on leaves, tested on fruits) outperforms the isolated *Momordica charantia* (MAE 4.58 vs. 7.60) under identical density.

While taxonomic priors offer useful guidance, visual cues remain critical. Evaluating the zero-shot approach GroundingREC [7] with taxonomic prompts yields a test MAE of 24.14 and R^2 of 0.53, falling behind visual-exemplar methods. Replacing LOCA’s ResNet-50 backbone with BioCLIP2 [17] also yields inferior results (MAE 34.75, R^2 0.29), likely because the low-resolution feature maps of ViT architectures without additional adapter designs are suboptimal for dense prediction. Since simple text encoding and off-the-shelf backbones underperform, moving beyond text to explicitly model inherent visual similarities among related species offers a promising path toward robust, fine-grained representations.

5. Conclusion

We present TPC-268, the first large-scale plant counting benchmark grounded in plant taxonomy. In contrast to prior counting datasets dominated by rigid or man-made objects, TPC-268 captures the hierarchical structure, morphological diversity, and multi-scale complexity of real-world plants. To assess its utility, we benchmark several representative CAC models and show incorporating plant taxonomic information is crucial for robust and generalizable counting in natural scenes. We hope TPC-268 will broaden the scope of visual counting research by challenging models to move beyond familiar regimes focused on rigid objects and by encouraging the development of representations to reason over fine grained structures and hierarchical organization.

For future work, we plan to extend TPC-268 with additional plant species, richer temporal and environmental annotations, and more biological organizational levels such as the cellular level to support biologically grounded counting.

Acknowledgement. This work is supported in part by the National Natural Science Foundation of China under Grant No. 62576146 and in part by the HUST Undergraduate Natural Science Foundation under Grant No. 62500034.

References

- [1] Niki Amini-Naieni, Tengda Han, and Andrew Zisserman. Countgd: Multi-modal open-world counting. *Adv. Neural Inf. Process. Syst.*, 37:48810–48837, 2024. 6, 7, 8
- [2] Carlos Arteta, Victor Lempitsky, and Andrew Zisserman. Counting in the wild. In *Proc. Eur. Conf. Comput. Vis.*, pages 483–498. Springer, 2016. 2, 3
- [3] Suchet Bargoti and James Underwood. Deep fruit detection in orchards. In *Proc. IEEE Int. Conf. Robot. Autom.*, pages 3626–3633. IEEE, 2017. 3
- [4] Thomas Borsch, Walter Berendsohn, Eduardo Dalcin, Maité Delmas, Sebsebe Demissew, Alan Elliott, Peter Fritsch, Anne Fuchs, Dmitry Geltman, Adil Güner, et al. World flora online: Placing taxonomists at the heart of a definitive and comprehensive global resource on the world’s plants. *Taxon*, 69(6):1311–1341, 2020. 4
- [5] Antoni B Chan, Zhang-Sheng John Liang, and Nuno Vasconcelos. Privacy preserving crowd monitoring: Counting people without people models or tracking. In *Proc. IEEE/CVF Conf. Comput. Vis. Pattern Recognit.*, pages 1–7. IEEE, 2008. 1
- [6] MyeongAh Cho, Minjung Kim, Sangwon Hwang, Chaewon Park, Kyungjae Lee, and Sangyoun Lee. Look around for anomalies: Weakly-supervised anomaly detection via context-motion relational learning. In *Proc. IEEE/CVF Conf. Comput. Vis. Pattern Recognit.*, pages 12137–12146, 2023. 1
- [7] Siyang Dai, Jun Liu, and Ngai-Man Cheung. Referring expression counting. In *Proceedings of the IEEE/CVF Conference on Computer Vision and Pattern Recognition*, pages 16985–16995, 2024. 8
- [8] Etienne David, Simon Madec, Pouria Sadeghi-Tehran, Helge Aasen, Bangyou Zheng, Shouyang Liu, Norbert Kirchgessner, Goro Ishikawa, Koichi Nagasawa, Minhajul A. Badhon, et al. Global wheat head detection (GWHD) dataset: A large and diverse dataset of high-resolution RGB-labelled images to develop and benchmark wheat head detection methods. *Plant Phenomics*, 2020:3521852, 2020. 2
- [9] Jia Deng, Wei Dong, Richard Socher, Li-Jia Li, Kai Li, and Li Fei-Fei. Imagenet: A large-scale hierarchical image database. In *Proc. IEEE/CVF Conf. Comput. Vis. Pattern Recognit.*, pages 248–255, 2009. 1
- [10] Andrei Dobrescu, Mario Valerio Giuffrida, and Sotirios A Tsafaris. Leveraging multiple datasets for deep leaf counting. In *Proceedings of the IEEE international conference on computer vision workshops*, pages 2072–2079, 2017. 3, 4
- [11] MR Ehsani, TE Grift, JM Maja, and D Zhong. Two fruit counting techniques for citrus mechanical harvesting machinery. *Comput. Electron. Agric.*, 65(2):186–191, 2009. 3
- [12] Mark Everingham, Luc Van Gool, Christopher K. I. Williams, John Winn, and Andrew Zisserman. The PASCAL visual object classes (VOC) challenge, 2010. 1
- [13] Karl C. Fetter, Sven Eberhardt, Rich S. Barclay, Scott Wing, and Stephen R. Keller. StomataCounter: A neural network for automatic stomata identification and counting. *New Phytol.*, 223(3):1671–1681, 2019. 2
- [14] Robert T Furbank and Mark Tester. Phenomics—technologies to relieve the phenotyping bottleneck. *Trends Plant Sci.*, 16(12):635–644, 2011. 3
- [15] Mario Valerio Giuffrida, Massimo Minervini, and Sotirios A Tsafaris. Learning to count leaves in rosette plants. In *Proc. Comput. Vis. Probl. Plant Phenotyping Workshop*. BMVA press, 2016. 3
- [16] Friederike Gnädinger and Urs Schmidhalter. Digital counts of maize plants by unmanned aerial vehicles (uavs). *Remote Sens.*, 9(6):544, 2017. 3
- [17] Jianyang Gu, Samuel Stevens, Elizabeth G Campolongo, Matthew J Thompson, Net Zhang, Jiaman Wu, Andrei Kopanev, Zheda Mai, Alexander E White, James Balhoff, et al. Bioclip 2: Emergent properties from scaling hierarchical contrastive learning. *arXiv preprint arXiv:2505.23883*, 2025. 8
- [18] Nicolai Häni, Pravakar Roy, and Volkan Isler. MinneApple: A benchmark dataset for apple detection and segmentation. *IEEE Robot. Autom. Lett.*, 5(2):1144–1151, 2020. 2
- [19] Shenghua He, Kyaw Thu Minn, Lilianna Solnica-Krezel, Mark A Anastasio, and Hua Li. Deeply-supervised density regression for automatic cell counting in microscopy images. *Med. Image Anal.*, 68:101892, 2021. 3
- [20] Meng-Ru Hsieh, Yen-Liang Lin, and Winston H Hsu. Drone-based object counting by spatially regularized regional proposal network. In *Proc. IEEE/CVF Int. Conf. Comput. Vis.*, pages 4145–4153, 2017. 1, 2, 3
- [21] Xiaonan Hu, Xuebing Li, Jinyu Xu, Abdulkadir Duran Adan, Letian Zhou, Xuhui Zhu, Yanan Li, Wei Guo, Shouyang Liu, Wenzhong Liu, et al. TasselNetV4: A vision foundation model for cross-scene, cross-scale, and cross-species plant counting. *arXiv preprint arXiv:2509.20857*, 2025. 6, 7
- [22] Haroon Idrees, Muhammad Tayyab, Kishan Athrey, Dong Zhang, Somaya Al-Maadeed, Nasir Rajpoot, and Mubarak Shah. Composition loss for counting, density map estimation and localization in dense crowds. In *Proc. Eur. Conf. Comput. Vis.*, pages 532–546, 2018. 2, 3
- [23] Alexis Joly, Pierre Bonnet, Hervé Goëau, Julien Barbe, Souheil Selmi, Julien Champ, Samuel Dufour-Kowalski, Antoine Affouard, Jennifer Carré, Jean-François Molino, et al. A look inside the pl@ ntnet experience: The good, the bias and the hope. *Multimedia Systems*, 22(6):751–766, 2016. 4
- [24] Satish Kumar, Bowen Zhang, Chandrakanth Gudavalli, Connor Levenson, Lacey Hughey, Jared A Stabach, Irene Amoke, Gordon Ojwang, Joseph Mukeka, Stephen Mwiu, et al. Wildlifemapper: Aerial image analysis for multi-species detection and identification. In *Proc. IEEE/CVF Conf. Comput. Vis. Pattern Recognit.*, pages 12594–12604, 2024. 3
- [25] Xin Li, Pinzhe Li, Xinzhe Wang, Yaning Zhu, Tianqi Hu, Binghui Xu, Yongshuai Zhang, Zhiguo Han, and Hao Lu. Cornpheno: Phenotyping corn ear kernels in the wild via point query transformer. *Plant Phenomics*, page 100129, 2025. 4

- [26] Yinglun Li, Xiaohai Zhan, Shouyang Liu, Hao Lu, Ruibo Jiang, Wei Guo, Scott Chapman, Yufeng Ge, Benoit Solan, Yanfeng Ding, and Frédéric Baret. Self-supervised plant phenotyping by combining domain adaptation with 3D plant model simulations: Application to wheat leaf counting at seedling stage. *Plant Phenomics*, 5:0041, 2023. 2
- [27] Tsung-Yi Lin, Michael Maire, Serge Belongie, James Hays, Pietro Perona, Deva Ramanan, Piotr Dollár, and C. Lawrence Zitnick. Microsoft coco: Common objects in context. In *Proc. Eur. Conf. Comput. Vis.*, pages 740–755. Springer International Publishing, 2014. 1
- [28] Wei Lin, Kunlin Yang, Xinzhu Ma, Junyu Gao, Lingbo Liu, Shinan Liu, Jun Hou, Shuai Yi, and Antoni B Chan. Scale-prior deformable convolution for exemplar-guided class-agnostic counting. In *Proc. Brit. Mach. Vis. Conf.*, page 313, 2022. 3, 6, 7
- [29] Carolus Linnaeus. *Systema Naturae per regna tria naturae, secundum classes, ordines, genera, species; cum characteribus, differentiis, synonymis, locis.* apud JB Delamolliere, 1789. 4
- [30] IUCN Red List. IUCN red list, 2011. 4
- [31] Chang Liu, Yujie Zhong, Andrew Zisserman, and Weidi Xie. Countr: Transformer-based generalised visual counting. In *Proc. Brit. Mach. Vis. Conf.*, 2022. 3, 6, 7
- [32] Shuai Liu, Peng Zhang, Shiwei Zhang, and Wei Ke. Countse: Soft exemplar open-set object counting. In *Proc. IEEE/CVF Int. Conf. Comput. Vis.*, pages 21536–21546, 2025. 3
- [33] Erika Lu, Weidi Xie, and Andrew Zisserman. Class-agnostic counting. In *Proc. Asian Conf. Comput. Vis.*, pages 669–684. Springer, 2018. 3, 6
- [34] Hao Lu, Zhiguo Cao, Yang Xiao, Bohan Zhuang, and Chunhua Shen. Tasselnet: counting maize tassels in the wild via local counts regression network. *Plant Methods*, 13:1–17, 2017. 1, 2, 3
- [35] Hao Lu, Liang Liu, Ya-Nan Li, Xiao-Ming Zhao, Xi-Qing Wang, and Zhi-Guo Cao. Tasselnetv3: Explainable plant counting with guided upsampling and background suppression. *IEEE Trans. Geosci. Remote Sens.*, 60:1–15, 2021. 4
- [36] Joe D. Luck, Santosh K. Pitla, and Scott A. Shearer. Sensor ranging technique for determining corn plant population. In *Proc. ASABE Annu. Int. Meet.*, 2008. 3
- [37] Laurens van der Maaten and Geoffrey Hinton. Visualizing data using t-SNE. *J. Mach. Learn. Res.*, 9(Nov):2579–2605, 2008. 7
- [38] Mark Marsden, Kevin McGuinness, Suzanne Little, Ciara E Keogh, and Noel E O’Connor. People, penguins and petri dishes: Adapting object counting models to new visual domains and object types without forgetting. In *Proc. IEEE/CVF Conf. Comput. Vis. Pattern Recognit.*, pages 8070–8079, 2018. 2, 3
- [39] Giulio Martellucci, Herve Goeau, Pierre Bonnet, Fabrice Vinatier, and Alexis Joly. Overview of plantclef 2025: Multi-species plant identification in vegetation quadrat images. *arXiv preprint arXiv:2509.17602*, 2025. 4
- [40] Massimo Minervini, Andreas Fischbach, Hanno Scharr, and Sotirios A Tsaftaris. Finely-grained annotated datasets for image-based plant phenotyping. *Pattern Recognit. Lett.*, 81: 80–89, 2016. 2
- [41] Thanh Nguyen, Chau Pham, Khoi Nguyen, and Minh Hoai. Few-shot object counting and detection. In *Proc. Eur. Conf. Comput. Vis.*, pages 348–365. Springer, 2022. 3, 6, 7
- [42] Jer Pelhan, Vitjan Zavrtanik, Matej Kristan, et al. Dave—a detect-and-verify paradigm for low-shot counting. In *Proc. IEEE/CVF Conf. Comput. Vis. Pattern Recognit.*, pages 23293–23302, 2024. 6, 7
- [43] Viresh Ranjan, Udbhav Sharma, Thu Nguyen, and Minh Hoai. Learning to count everything. In *Proc. IEEE/CVF Conf. Comput. Vis. Pattern Recognit.*, pages 3393–3402, 2021. 3, 4, 6, 7
- [44] Caroline A Schneider, Wayne S Rasband, and Kevin W Elceiri. Nih image to imagej: 25 years of image analysis. *Nat. Methods*, 9(7):671–675, 2012. 3
- [45] Min Shi, Hao Lu, Chen Feng, Chengxin Liu, and Zhiguo Cao. Represent, compare, and learn: A similarity-aware framework for class-agnostic counting. In *Proc. IEEE/CVF Conf. Comput. Vis. Pattern Recognit.*, pages 9529–9538, 2022. 3, 6, 7
- [46] Vishwanath A Sindagi, Rajeev Yasarla, and Vishal M Patel. Jhu-crowd++: Large-scale crowd counting dataset and a benchmark method. *IEEE Trans. Pattern Anal. Mach. Intell.*, 44(5):2594–2609, 2020. 2, 3
- [47] Guolei Sun, Zhaochong An, Yun Liu, Ce Liu, Christos Sakaridis, Deng-Ping Fan, and Luc Van Gool. Indiscernible object counting in underwater scenes. In *Proc. IEEE/CVF Conf. Comput. Vis. Pattern Recognit.*, 2023. 2, 3
- [48] Takanari Tanabata, Taeko Shibaya, Kiyosumi Hori, Kaworu Ebana, and Masahiro Yano. Smartgrain: high-throughput phenotyping software for measuring seed shape through image analysis. *Plant Physiol.*, 160(4):1871–1880, 2012. 3
- [49] Nikola Đukić, Alan Lukežič, Vitjan Zavrtanik, and Matej Kristan. A low-shot object counting network with iterative prototype adaptation. In *Proc. IEEE/CVF Int. Conf. Comput. Vis.*, pages 18872–18881, 2023. 6, 7, 8
- [50] Grant Van Horn, Oisín Mac Aodha, Yang Song, Yin Cui, Chen Sun, Alex Shepard, Hartwig Adam, Pietro Perona, and Serge Belongie. The iNaturalist species classification and detection dataset. In *Proc. IEEE/CVF Conf. Comput. Vis. Pattern Recognit.*, pages 8769–8778, 2018. 2
- [51] Jihong Wang, Heidi J Renninger, and Qingmin Ma. Labeled temperate hardwood tree stomatal image datasets from seven taxa of *Populus* and 17 hardwood species. *Sci Data*, 11:1, 2024. 4
- [52] Qi Wang, Junyu Gao, Wei Lin, and Xuelong Li. NWPU-Crowd: A large-scale benchmark for crowd counting and localization. *IEEE Trans. Pattern Anal. Mach. Intell.*, 2020. 3
- [53] Zhicheng Wang, Liwen Xiao, Zhiguo Cao, and Hao Lu. Vision transformer off-the-shelf: A surprising baseline for few-shot class-agnostic counting. In *Proc. AAAI Conf. Artif. Intell.*, pages 5832–5840, 2024. 3, 6, 7
- [54] Douglas W Whitman, Anurag A Agrawal, et al. What is phenotypic plasticity and why is it important. *Phenotypic Plasticity of Insects: Mechanisms and Consequences*, pages 1–63, 2009. 1
- [55] Zhiyuan You, Kai Yang, Wenhan Luo, Xin Lu, Lei Cui, and Xinyi Le. Few-shot object counting with similarity-aware

- feature enhancement. In *Proc. IEEE Winter Conf. Appl. Comput. Vis.*, pages 6315–6324, 2023. [3](#), [6](#), [7](#)
- [56] Yingying Zhang, Desen Zhou, Siqin Chen, Shenghua Gao, and Yi Ma. Single-image crowd counting via multi-column convolutional neural network. In *Proc. IEEE/CVF Conf. Comput. Vis. Pattern Recognit.*, pages 589–597, 2016. [1](#), [2](#), [3](#)

Plant Taxonomy Meets Plant Counting: A Fine-Grained, Taxonomic Dataset for Counting Hundreds of Plant Species

Supplementary Material

The supplementary material provides the algorithms for dataset partitioning, the method for mapping the hierarchical taxonomic structure, qualitative visualizations and some image examples. First, **Sec. A** details the Mixed-Integer Linear Programming (MILP) formulation for dataset partitioning. Second, **Sec. B** explains how we construct the mapping from taxonomic names to hierarchical codes. Finally, **Sec. C** presents both qualitative comparisons with baselines and diverse visual examples.

A. MILP-based Dataset Partitioning

We propose a Mixed-Integer Linear Programming (MILP) approach to partition the dataset. This ensures taxonomic independence between subsets while maintaining statistical balance in instance density.

A.1. Process Description

The pipeline consists of three stages:

Build Units. We group images into atomic units based on unique *Species-Organization* pairs. For example, all images of *Zea mays-flower* form a single unit. Each atomic unit corresponds to a unique visual phenotype of a single species and is assigned exclusively to one subset.

Optimize Assignments. The unit assignments are determined using the PULP_CBC_CMD solver. The optimization objective combines two types of deviation penalties. First, we minimize how far the image counts (\hat{N}_k) deviate from the target 7 : 1 : 2 proportion, ensuring that the group sizes remain close to this desired ratio. Second, we minimize the imbalance in the average number of object instances (points) (\hat{P}_k) across groups. Since matching the image ratio is more important, we assign it a much larger weight ($\lambda_{img} = 100.0$) compared to the weight for balancing instance counts ($\lambda_{pts} = 1.0$). This forces the solver to satisfy the image ratio first, and only then adjust the instance distribution.

Ensure Coverage. To ensure that the model is exposed to all levels of biological organization, we enforce a hard constraint that the training split must include at least one unit from every category. After the solver completes, we also verify that each of the three subsets contains data from all observation scales (Microscopy, Close-range, Remote Sensing). If any subset lacks a particular scale, the partition is rejected and the optimization is restarted with a different random seed for the solver’s internal heuristics, ensuring a new search trajectory and a fresh candidate solution.

A.2. Problem Formulation

Let \mathcal{D} be the full dataset containing images I , and let $\mathcal{U} = \{u_1, \dots, u_M\}$ denote the set of atomic units, where each unit corresponds to a unique *Species-Organization* pair. For each unit u , we denote by n_u the number of images and by p_u the total number of object instances.

Let \mathcal{O} be the set of biological organization categories, and let $\mathcal{U}_o \subseteq \mathcal{U}$ denote the units belonging to category o . Similarly, let \mathcal{T} be the set of observation scales (Microscopy, Close-range, Remote Sensing), and let $\mathcal{U}_t \subseteq \mathcal{U}$ denote the units originating from scale t .

We partition \mathcal{U} into three subsets $\mathcal{S} = \{\text{train, val, test}\}$ with target proportions $r_k = \{0.7, 0.1, 0.2\}$.

Decision Variables. For each unit u and split k , we define a binary assignment variable:

$$x_{u,k} = \begin{cases} 1, & \text{if unit } u \text{ is assigned to split } k, \\ 0, & \text{otherwise.} \end{cases}$$

Objective Function. We minimize the weighted deviation between the actual and target totals for image counts (\hat{N}_k) and point counts (\hat{P}_k). The objective function is formulated as:

$$\min \sum_{k \in \mathcal{S}} \left(\lambda_{img} \left| \sum_{u \in \mathcal{U}} n_u x_{u,k} - \hat{N}_k \right| + \lambda_{pts} \left| \sum_{u \in \mathcal{U}} p_u x_{u,k} - \hat{P}_k \right| \right) \quad (1)$$

where $\hat{N}_k = r_k \sum_u n_u$ and $\hat{P}_k = r_k \sum_u p_u$. We use $\lambda_{img} = 100$ and $\lambda_{pts} = 1$ to strictly prioritize the adherence to the image-count ratio.

Constraints. The optimization is subject to the following constraints:

- i) *Unique assignment.* Each unit must be assigned to exactly one split:

$$\sum_{k \in \mathcal{S}} x_{u,k} = 1, \quad \forall u \in \mathcal{U}. \quad (2)$$

- ii) *Training set coverage.* To ensure robust feature learning, the training subset is explicitly constrained to in-

clude at least one unit from each organization category:

$$\sum_{u \in \mathcal{U}_o} x_{u,\text{train}} \geq 1, \quad \forall o \in \mathcal{O}. \quad (3)$$

Verification. While the MILP guarantees organization coverage for the training set, we additionally require that all splits cover the full spectrum of observation scales. After optimization, we verify that:

$$\sum_{u \in \mathcal{U}_t} x_{u,k} \geq 1, \quad \forall t \in \mathcal{T}, \forall k \in \mathcal{S}. \quad (4)$$

If this condition is not met for any split k , the resulting partition is discarded, and the optimization is re-initialized with a different random seed until a valid solution is obtained.

B. Hierarchical Taxonomic Encoding

We follow the standard 7-hierarchy biological taxonomy—*Kingdom, Phylum, Class, Order, Family, Genus, and Species*. To build the index mappings, we first sort all species names in the dataset and iterate through them in order. For each species, we retrieve its taxonomic labels across all remaining hierarchies. Whenever a hierarchy encounters a category name for the first time, we append it to that level’s dictionary and assign the next integer index starting from 1. Formally, for each hierarchy h , this procedure defines a mapping

$$\phi_h : \mathcal{C}_h \rightarrow \{1, 2, \dots, |\mathcal{C}_h|\},$$

where \mathcal{C}_h denotes the set of unique category names observed at hierarchy h . This construction yields a complete mapping from taxonomic names to integer identifiers for every hierarchy.

Under this protocol, each species is encoded as a 7-dimensional vector v :

$$v = [id_{\text{king}}, id_{\text{phy}}, id_{\text{cls}}, id_{\text{ord}}, id_{\text{fam}}, id_{\text{gen}}, id_{\text{spec}}]$$

where each component id indicates the integer index of the taxon at that specific hierarchy.

Example. Consider the species *Malus domestica*. Its taxonomic path maps to the following indices:

Kingdom: *Plantae* \rightarrow 1; Phylum: *Tracheophyta* \rightarrow 1; Class: *Magnoliopsida* \rightarrow 1; Order: *Rosales* \rightarrow 14; Family: *Rosaceae* \rightarrow 39; Genus: *Malus* \rightarrow 113; Species: *Malus domestica* \rightarrow 136.

Consequently, the hierarchical encoding vector is:

$$v_{\text{Malus domestica}} = [1, 1, 1, 14, 39, 113, 136]$$

The file `taxonomy_ids.json` contains the complete index mappings for all categories across all 7 taxonomic

hierarchies. This file is included with the supplementary materials, and its structure is illustrated below:

```
{
  "Kingdom": {
    "Plantae": 1,
    "Fungi": 2
  },
  "Phylum": {
    "Tracheophyta": 1,
    "Basidiomycota": 2
  },
  ...
  "Family": {
    "Malvaceae": 1,
    "Fabaceae": 2,
    ...
    "Rhamnaceae": 83
  },
  ...
  "Species": {
    "Abelmoschus esculentus": 1,
    ...
    "Zea mays": 240,
    "Ziziphus mauritiana": 242
  }
}
```

C. Visualizations and Examples

Fig. 7 shows images of a single species observed at different growth stages, where the changes in plant size, structure, and overall appearance become clearly visible across the timeline.

Fig. 8 presents examples from several biological organizations of the same species. The differences in texture, geometry, and visual scale across tissues, organs, and whole plants are evident from these samples.

Fig. 9 includes images collected under low-light conditions. Reduced visibility and unstable illumination make object boundaries harder to distinguish.

Fig. 10 shows real-world scenes, with irregular backgrounds, occlusions, and surrounding environment adding substantial visual clutter.

Fig. 11 provides representative high-density cases containing large numbers of closely arranged instances. The crowded layouts and overlapping structures make accurate separation and counting particularly difficult.

As shown in Fig. 12, we include qualitative comparisons across multiple baseline methods to illustrate their performance under different plant-counting conditions.



Figure 7. **Examples of the same species at different growth stages in our TPC-268.** The images span early seedling, vegetative development, tasseling, and final maturity.



Figure 8. **Examples of different biological organizations from the same species in our TPC-268.** Tissue-level, organ-level, and whole-plant-level images show distinct texture patterns and structural characteristics.



Figure 9. **Examples of images captured in dark or low-illumination environments from our TPC-268.** Reduced contrast, color distortion, and shadow-induced ambiguity complicate instance perception.



Figure 10. **Examples of real-world scenarios in our TPC-268.** Natural backgrounds, occluding structures, and cluttered surroundings reflect practical field conditions.



Figure 11. **Examples of high-density counting scenarios in our TPC-268.** These images include scenes containing hundreds or even thousands of instances, characterized by compact spatial arrangement, heavy overlap, and minimal inter-instance separation.

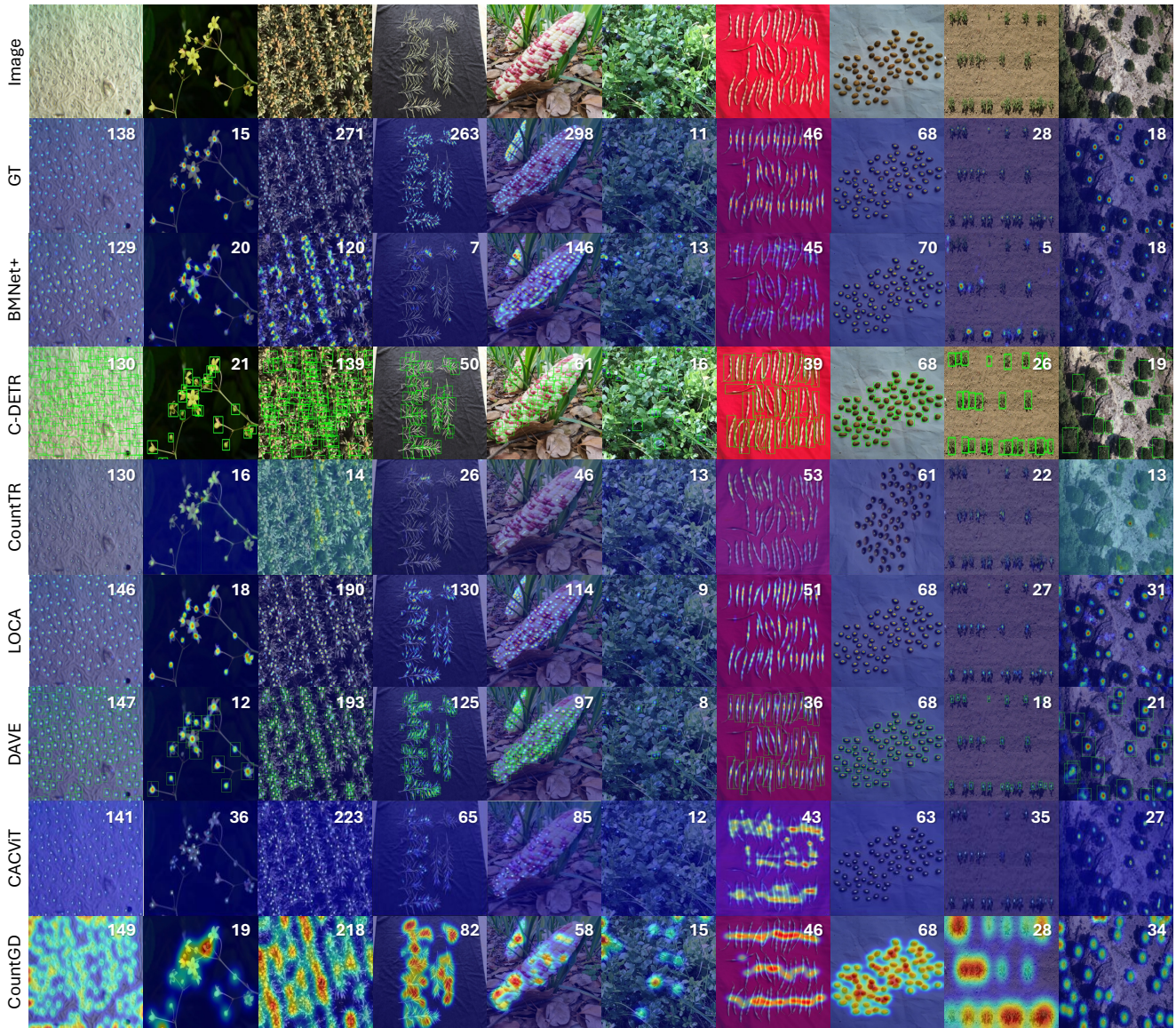


Figure 12. **Qualitative results of representative counting methods on our TPC-268.** The examples cover diverse plant forms, observation scales, and density levels.